QUASI 3D REFINED SIMULATION OF FLOW AND POLLUTANT TRANSPORT IN THE YANGTZE RIVER

Li-ren Yu[1]

[1]*ESDV (Environmental Software and Digital Visualization), Wan-Sheng-Bei-Li, Ton-Zhou Dist.,China, ASSER-CESUSC*

(Association of United Schools-Higher Education Center at São Carlos), Brazil

ABSTRACT

This paper reports a quasi 3D simulation in a curved river reach of The Yangtze River near The Huangshigang City, aiming to develop a numerical tool for modeling turbulent flows and pollutant transport in complex natural waters. The depth-averaged two-equation turbulence $\widetilde{k} - \widetilde{\omega}$ model, together with $\widetilde{k} - \widetilde{\varepsilon}$ and $\widetilde{k} - \widetilde{w}$ models, were used to close quasi 3D hydrodynamic fundamental governing equations. The discretized equations were solved by advanced multi-grid iterative method under coarse and fine two-levels' grids. The processes of plume development, caused by the side-discharge from a tributary, also have been investigated numerically. The used three turbulence models are suitable for modeling strong mixing turbulence. The $\widetilde{k} - \widetilde{\omega}$ model with higher order of magnitude of transported variable $\widetilde{\omega}$ provides a possibility to increase the computational precision. Based on the developed hydrodynamic model, a CFD software, namely **Q3drm1.0**, was preliminarily developed. This tool focuses on the refined simulations of the steady and unsteady problems of flow and transports with the strong ability to treat different types of discharges.

Keywords: Depth-averaged turbulence models, Contaminant transport, River modeling, Curved River, Numerical modeling, Multi-grid iterative method.

Contribution/ Originality

This study is one of very few studies which have numerically investigated the flow and pollutant transport caused by the side discharge in The Yangtze River, by using three depth-averaged two-equation closure turbulence models and multi-grid iterative method, with the aim to develop a quasi 3D modeling CFD software.

1. INTRODUCTION

Almost all flows in rivers are turbulence. Dealing with the problems of turbulence tightly related to stream pollutions is challenging both for scientists and engineers, because of their damaging effect on our fragile environment and limited water resources. It is important to develop adequate mathematical models, turbulence closure models, numerical methods and tools for timely simulating and predicting contaminant transport behaviors in natural and artificial waters.

Although the significance of modeling turbulent flows and transport phenomena with a high precision is clear, the numerical simulation and prediction for natural waters with complex geometry are still unsatisfied. This is mainly due to the inherent complexity of the problems being considered. Any computation and simulation of flow and transport processes critically depends on four elements: to generate a suitable computational domain with the ability to deal with non-regular geometrical boundaries, such as meandering riversides and island boundaries; to establish practical turbulence closure models; to adopt efficient computational method and algorithm, and to develop numerical tool, respectively.

Many environmental flows can be considered as shallow, *i.e.*, the horizontal length scales of the flow domain are much larger than the water-depth. Typical examples are often found in lakes, lowland rivers and coastal areas. Depth-averaged mathematical models are frequently used for modeling the flow and contaminant transport in well-mixed shallow waters. However, many models used in practice merely consider the depth-averaged turbulent viscosity and diffusivity through constants or through simple phenomenological algebraic formulas [1-5] which are estimated to a great degree according to the modeler's experience. Although some practical quasi 3D hydrodynamic models are really closed by depth-averaged two-equation closure turbulence model, they almost all concentrate on the investigations and applications of depth-averaged $\widetilde{k} - \widetilde{\varepsilon}$ model [6-13] which appeared already beyond 30 years. It is well known that the order of magnitude of transported variable $\widetilde{\varepsilon}$ of $\widetilde{k} - \widetilde{\varepsilon}$ model is very low indeed. Recent development of turbulence modeling theory has provided more realistic turbulence closure models. From an engineering perspective, two-equation closure turbulence models can build a higher standard for numerically approximation of main flow behaviors and transport phenomena in terms of efficiency, extensibility and robustness [14]. Unfortunately, the 'standard' two-equation closure models, used widely in industry, cannot be directly employed in quasi 3D modeling. The depth-averaged turbulence models should be established in advance. Except for the newly established depth-averaged $\widetilde{k} - \widetilde{\omega}$ model closure, current simulations still adopt the closure approaches of classical $\widetilde{k} - \widetilde{\varepsilon}$ model and $\widetilde{k} - \widetilde{w}$ model, respectively. The $\widetilde{k} - \widetilde{\omega}$ model was stemmed from the

most common 'standard' k-ω mode. In this paper, the results, computed by the three depth-averaged two-equation turbulence models, were compared each other. Such example, however, hardly exists for the simulation of contaminant transport in natural waters. Modeling by using different two-equation closure approaches certainly increases the credibility of computational results [14].

On the other hand, recent advancements in grid generation, numerical methods and IT techniques have provided suitable approaches to generate non-orthogonal boundary-fitted coordinates with collocated grid arrangement, on which the non-simplified hydrodynamic fundamental governing equations can be solved by multi-grid iterative method [15]. This paper describes a quasi 3D hydrodynamic simulation of flow and contaminant transport in a curved river reach of The Yangtze River, with the aim to develop the *grid-generator*, *flow-solver* and GUI (*Graphical User Interface*). The developed Q3drm1.0 software, provides three selectable depth-averaged two-equation closure turbulence models, and can refinedly solve quasi 3D flow and contaminant transport phenomena in complex waters with or without islands, including bifurcated problem.

2. HYDRODYNAMIC FUNDAMENTAL GOVERNING EQUATIONS

The complete fundamental governing equations of quasi 3D computation for a Control Volume (CV, an arbitrary quadrilateral with center point P), considering the variation of the bottom topography and water surface and neglecting minor terms in the depth-averaging procedure, can be written as follows:

$$\frac{\partial}{\partial t}\int_{\Omega}\rho h\,\overline{\phi}\,d\Omega + \int_{S}\rho h\,\overline{\phi}\,\overrightarrow{v}\bullet\overrightarrow{n}dS = \int_{S}\Gamma h\,\mathbf{grad}\,\overline{\phi}\bullet\overrightarrow{n}dS + \int_{\Omega}\overline{q}_{\phi}d\Omega \tag{1}$$

where Ω is the CV's volume; S is the face; $\overrightarrow{v}$ is the depth-averaged velocity vector; the superscript "$^{-}$" indicates that the value is strictly depth-averaged; $\overline{\phi}$ is any depth-averaged conserved intensive property (for mass conservation, $\overline{\phi}=1$; for momentum conservation, $\overline{\phi}$ is the components in different directions of $\overrightarrow{v}$; for conservation of a scalar, $\overline{\phi}$ is the conserved property per unit mass); Γ is the diffusivity for the quantity $\overline{\phi}$; $\overline{q}_{\phi}$ denotes the source or sink of $\overline{\phi}$; and h and $\square$ are local water depth at P and density, respectively.

For the momentum conservation of Eq. (1), $\Gamma = \widetilde{\mu}_{\textit{eff}}$ (depth-averaged effective viscosity); for concentration transport, $\Gamma = \widetilde{\Gamma}_{\phi j}$ (concentration diffusivity), where the superscript "~" indicates the quantity characterizing depth-averaged turbulence. The source (sink) term $\overline{q}_{\phi}$ for momentum conservation may include surface wind shear stresses, bottom shear stresses, pressure terms and additional point sources (or point sinks).

3. DEPTH-AVERAGED TURBULENCE CLOSURE MODELS

The depth-averaged effective viscosity $\widetilde{\mu}_{\textit{eff}}$ and diffusivity $\widetilde{\Gamma}_{\phi j}$, appeared in Eq. (1), are dependent on the molecular dynamic viscosity μ and depth-averaged eddy viscosity $\widetilde{\mu}_{t}$:

$\widetilde{\mu}_{\textit{eff}} = \mu + \widetilde{\mu}_{t}$ and $\widetilde{\Gamma}_{\phi j} = \widetilde{\mu}_{t} / \sigma_{\phi j}$, where $\sigma_{\phi t}$ is the turbulence Schmidt number for concentration diffusion, and $\widetilde{\mu}_{t}$ is a scalar property and normally determined by two extra transported variables.

Recently, the author established a depth-averaged two-equation turbulence $\widetilde{k} - \widetilde{\omega}$ model based on the 'standard' k-ω model (in which ω is the special dissipation rate), originally introduced by Saffman [16] but popularized by Wilcox [17]. The 'standard' k-ω turbulence model has been used in engineering researches [18, 19]. In $\widetilde{k} - \widetilde{\omega}$ model, the turbulent viscosity is expressed by:

$$\widetilde{\mu}_{t} = \rho \widetilde{k} / \widetilde{\omega} \tag{2}$$

where $\widetilde{k}$ and $\widetilde{\omega}$ stand for the depth-averaged turbulent kinetic energy and special dissipation rate of $\widetilde{k}$. They are determined by solving two extra transport equations, $\textit{i.e.}$, the $\widetilde{k}$-eq. and $\widetilde{\omega}$-eq, respectively. [20]:

$$\frac{\partial(\rho h \widetilde{k})}{\partial t} + div(\rho h \widetilde{k} \widetilde{v}) = div(h(\mu + \frac{\widetilde{\mu}_{t}}{\sigma_{k}})\mathbf{grad}\,\widetilde{k}) + hP_{k} - \rho \beta^{*} h \widetilde{k} \widetilde{\omega} + \rho h P_{kv} + \overline{S}_{k} \tag{3}$$

$$\frac{\partial(\rho h \widetilde{\omega})}{\partial t} + div(\rho h \widetilde{\omega v}) = div(h(\mu + \frac{\widetilde{\mu}_t}{\sigma_\omega^*})\mathbf{grad}\,\widetilde{\omega}) + \alpha h \frac{\widetilde{\omega}}{\widetilde{k}} P_k - \rho h \beta \widetilde{\omega}^2 + \rho h P_{\omega v} + \overline{S}_\omega$$

(4)

$$P_k = \widetilde{\mu}_t \left[2\left(\frac{\partial \widetilde{u}}{\partial x}\right)^2 + 2\left(\frac{\partial \widetilde{v}}{\partial y}\right) + \left(\frac{\partial \widetilde{u}}{\partial y} + \frac{\partial \widetilde{v}}{\partial x}\right)^2 \right]$$

where $\overline{S}_k$ and $\overline{S}_\omega$ are the source-sink terms, is

the production of turbulent kinetic energy. The values of empirical constants α, $\square$, β^*, σ_k^*, and

σ_ω^* in Eq. (3) through Eq. (4) are the same as in the 'standard' k-ω model: 5/9, 0.075, 0.9, 2, and

2. According to the dimensional analysis, the additional source terms P_{kv} in k-eq. (3) and $P_{\omega v}$ in

ω-eq. (4) are mainly produced by the vertical velocity gradients near the bottom, and can be

expressed as follows:

$$P_{kv} = C_k u_*^3 / h, \ P_{\omega v} = C_\omega u_*^2 / h^2$$

(5)

while the local friction velocity u_* is equal to $\sqrt{C_f\left(\overline{u}^2 + \overline{v}^2\right)}$, the empirical constant C_ω for open

channel flow and rivers can be expressed as:

$$C_\omega = \beta / (C_\mu \times e^* \times C_f^{1/2})$$

(6)

where C_f represents an empirical friction factor and e^* is the dimensionless diffusivity of the

empirical formula for undisturbed channel/river flows $\widetilde{\mu}_t = e^* U_* h$ with U_* being the global

friction velocity.

Except for the newly developed $\widetilde{k} - \widetilde{\omega}$ turbulence model mentioned above, the author also

uses depth-averaged $\widetilde{k} - \widetilde{\varepsilon}$ model and $\widetilde{k} - \widetilde{w}$ model, to close the fundamental governing

equations in the current computations. The $\widetilde{k} - \widetilde{\varepsilon}$ model was suggested by McGuirk and Rodi

[21] as early as in 1977:

$$\frac{\partial(\rho h \widetilde{k})}{\partial t} + div(\rho h \widetilde{k v}) = div(h(\mu + \frac{\widetilde{\mu}_t}{\sigma_k})\mathbf{grad}\,\widetilde{k}) + h P_k - \rho h \widetilde{\varepsilon} + \rho h P_{kv} + \overline{S}_k$$

(7)

$$\frac{\partial(\rho h \widetilde{\varepsilon})}{\partial t} + div(\rho h \widetilde{\varepsilon v}) = div(h(\mu + \frac{\widetilde{\mu}_t}{\sigma_\varepsilon})\mathbf{grad}\,\widetilde{\varepsilon}) + C_1 h P_k \frac{\widetilde{\varepsilon}}{\widetilde{k}} - C_2 \rho h \frac{\widetilde{\varepsilon}^2}{\widetilde{k}} + \rho h P_{\varepsilon v} + \overline{S}_\varepsilon$$

(8)

where $\overline{S}_k$ and $\overline{S}_\varepsilon$ are the source-sink terms, $\widetilde{\mu}_t$ can be expressed as:

$$\widetilde{\mu}_t = \rho C_\mu \widetilde{k}^2 / \widetilde{\varepsilon} \tag{9}$$

where $\widetilde{\varepsilon}$ stands for dissipation rate of $\widetilde{k}$. The values of empirical constants C_μ, σ_k, σ_ε, C_1

and C_2 in Eqs. (7-9) are the same as the 'standard' k-ε model, *i.e.* equal to 0.09, 1.0, 1.3, 1.44 and 1.92, respectively. The additional source terms P_{kv} and $P_{\varepsilon v}$ in Eqs. (7) and (8) can be written by:

$$P_{kv} = C_k u_*^3 / h \, , \; P_{\varepsilon v} = C_\varepsilon u_*^4 / h^2 \tag{10}$$

where the empirical constants C_k and C_ε for open channel flow and rivers are:

$$C_k = 1 / \sqrt{C_f} \, , \; C_\varepsilon = C_2 C_\mu^{1/2} / (C_f^{3/4} \times e^{\bullet 1/2}) \tag{11}$$

The third used depth-averaged second-order closure $\widetilde{k} - \widetilde{w}$ model was previously developed by the author of the present paper and his colleague [22]. This model originated from the revised k-w model developed by Ilegbusi and Spalding [23]. The two extra transport equations of this model (*i.e.*, the $\widetilde{k}$-eq. and the $\widetilde{w}$-eq.) should be:

$$\frac{\partial(\rho h \widetilde{k})}{\partial t} + div(\rho h \widetilde{k} \overline{v}) = div(h(\mu + \frac{\widetilde{\mu}_t}{\sigma_k})\mathbf{grad}\widetilde{k}) + h P_k + \rho h P_{kv} - C_\mu \rho h \widetilde{k} \widetilde{w}^{1/2} + \overline{S}_k \tag{12}$$

$$\frac{\partial(\rho h \widetilde{w})}{\partial t} + div(\rho h \widetilde{w} \overline{v}) = div(h(\mu + \frac{\widetilde{\mu}_t}{\sigma_\varepsilon})\mathbf{grad}\widetilde{w}) + C_{1w}\widetilde{\mu}_t h(\mathbf{grad}\,\Omega)^2$$

$$- C_{2w} \rho h \widetilde{w}^{3/2} f + C_{3w} h \frac{\widetilde{w}}{\widetilde{k}} P_k + \rho h P_{wv} + \overline{S}_w \tag{13}$$

where $\overline{S}_k$ and $\overline{S}_w$ are the source-sink terms; function $f = 1 + C'_{2w}\left(\partial L / \partial x_i\right)$ and L is the characteristic distance of turbulence; Ω stands for mean movement vorticity. In $\widetilde{k} - \widetilde{w}$ model, the turbulent viscosity is defined as:

$$\widetilde{\mu}_t = \rho \widetilde{k} / \widetilde{w}^{1/2} \tag{14}$$

where $\widetilde{w}$ is depth-averaged time-mean-square vorticity fluctuation of turbulence. The transport equations (the $\widetilde{k}$-eq. and $\widetilde{w}$-eq.) should be also solved in this model. The values of empirical constants C_μ, σ_k, σ_w, C_{lw}, C_{2w}, C'_{2w} and C_{3w} are the same as those of 'standard' k-w model, *i.e.*, equal 0.09, 1.0, 1.0, 3.5, 0.17, 17.47 and 1.12, respectively. The corresponding additional source terms P_{kv} and P_{wv}, also mainly due to the vertical velocity gradients near the bottom, and can be expressed as:

$$P_{kv} = C_k u_*^3 / h, \; P_{wv} = C_w u_*^3 / h^3 \tag{15}$$

The empirical constants C_w for open channel flow and rivers can be written as:

$$C_w = C_{2w} / \left(C_\mu^{3/2} \times C_f^{3/4} \times e^{\bullet 3/2} \right) \tag{16}$$

The mathematical model and turbulence models, developed by the author, have been numerically investigated with laboratorial and site data for different flow situations [22, 24]. In the established mathematical model, the original empirical constants of three turbulence models, suggested by their authors, are employed and do not been changed never.

Figure 1 displays a comparison of computational example between the fine light-blue concentration contour with $35 mg/L$, calculated by using $\widetilde{k} - \widetilde{\varpi}$ model closure and plotted by **Q3drm1.0**, and the outline of black-water plume, shown on the *Google* satellite map. In this computation, one reach of the Amazon River near The Manaus City, Brazil, has been computed, where The Negro River flows into The Solimões River from the North and the West to form The Amazon River below this city. The confluent tributaries in the Amazon's water system usually have concentration difference in comparison with the mainstream, caused by the humus in tropical rain forest. The Negro River, however, is the largest left tributary of The Amazon and the largest black-water river in the world. In this figure, the coarse yellow lines demonstrate the outline of computational domain and islands. It is clear that the simulated depth-averaged concentration contour, however, is well coincident with the outline of black-water plume.

Fig-1. Comparison between calculated concentration contour and black-water plume outline [14].

4. GRID GENERATION

In this paper, one curved reach of The Yangtze River, China, has been computed by using the *grid-generator* and *flow-solver*, where a small tributary flows into the river from its left bank. The confluent tributary has a concentration difference in comparison with the mainstream. With the help of the developed software, it is possible to determine the scale of digital map, to collect geometrical data, including the positions of two curved riversides, four boundaries of two islands and the location of confluent tributary section, and finally to generate one text file. In this file, all of messages, which illustrate necessary control variables and characteristic parameters are contained, and can be read by *grid-generator* to generate the expectant coarse and fine two levels' grids.

Fig-2. *Google* map, plotted by interface.
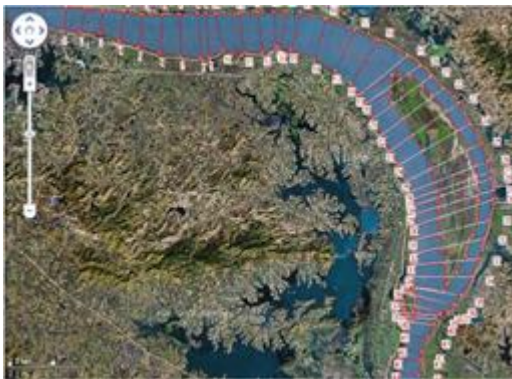
Fig-3. Coarse grid.

Fig-4. Fine grid.

Fig-5. Bottom topography.
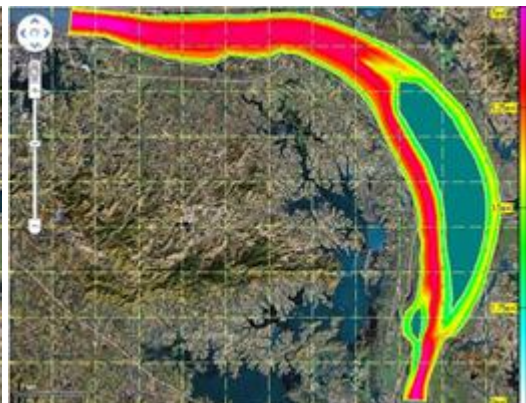
Figure 2 demonstrates the digital map, on which the developed *interface* of **Q3drm1.0** has divided the computational river reach into 43 sub-reaches with 44 short cross-river lines. Figure 3 presents the generated body-fitted non-orthogonal coarse gridwith the resolution of 130 nodal points in *i*-direction and 18 points in *j*-direction, respectively. In the generated mesh, the nodal

points on transversal grid lines are uniform. The total length of the calculated river reach is $31.34\,km$. The flow direction is from the West to the South. The tributary feeds into the mainstream on the north riverside with the numbers of nodal points at i from 97 to 98 on the coarse grid. The developed *grid-generator* generated two layers' grids, on which all of geometric data, necessary in the later calculation of flow and contaminant transport, must be stored and then can be read by the developed *flow-solver*. The resolution of the fine grid is 258×34, displayed on Figure 4. Figure 5 represents the bottom topography on coarse grid. During the calculation, the variation of bottom topography was considered. On Figures 3-5, the interval between two horizontal and vertical coordinate lines is $2\,km$.

5. SOLUTIONS OF FLOW AND SIDE DISCHARGE

The behaviors of flows and transport were simulated by using the developed *flow-solver*, in which the SIMPLE algorithm for FVA, Guass' divergence theorem, ILU decomposition, PWIM, SIP, under relaxation and multi-grid iterative method have been used. The hydrodynamic fundamental governing equations were solved firstly at the coarse grid and then at the fine grid, in the following sequence for each grid level: two momentum equations ($\overline{u}$-eq. and $\overline{v}$-eq.), one pressure-correction equation (p'-eq.), one concentration transport equation ($\overline{C_1}$-eq.), and two transport equations $\widetilde{k}\text{-}\widetilde{\varepsilon}$ $\widetilde{k}\text{-}\widetilde{w}\text{-}\widetilde{k}$ $\widetilde{\omega}$, respectively.

The calculated main stream flow-rate is $10{,}000\,m^3/s$, while the width, area and mean water-depth of the inlet section are $1{,}154.86\,m$, $5{,}797\,m^2$ and $5.71\,m$. The empirical friction factor (C_f) equals 0.00244. The flow-rate and concentration difference of tributary are $100\,m^3/s$ and $100\,mg/L$, respectively. Three depth-averaged two-equation closure turbulence models, *i.e.*, the $\widetilde{k}-\widetilde{\varepsilon}$, $\widetilde{k}-\widetilde{w}$ and $\widetilde{k}-\widetilde{\omega}$, are adopted to close the quasi 3D hydrodynamic model. The turbulent variables at the inlet sections can be calculated by empirical formulae, *i.e.*, $\widetilde{k}_0$, $\widetilde{\varepsilon}_0$, $\widetilde{w}_0$, $\widetilde{\omega}_0$ are $0.065\,m^2/s^2$, $0.00148\,m^2/s^3$, $0.368/s^2$, $0.254/s$, and $\widetilde{k}_{ri}$, $\widetilde{\varepsilon}_{ri}$, $\widetilde{w}_{ri}$, $\widetilde{\omega}_{ri}$ equal $0.046\,m^2/s^2$, $0.00115\,m^2/s^3$, $0.152/s^2$, $0.275/s$, respectively. On the outlet section, the variables satisfy constant gradient condition. The wall function approximation was used for determining the values of velocity components and turbulent variables at the nodal points in the vicinity of riversides and islands' boundaries.

The simulation obtained various 2D and 3D distributions of flow, pressure, concentration and turbulent variables and parameters, which are useful to analyze interested problems in engineering.

Q3drm1.0 provides powerful browsers for plotting and analyzing computational results. A part of results, simulated by using $\widetilde{k}-\widetilde{\varepsilon}$, $\widetilde{k}-\widetilde{w}$ and $\widetilde{k}-\widetilde{\omega}$ models on the fine grid, are presented from Figure 6 to Figure 10. Figure 6 display the results, calculated by using $\widetilde{k}-\widetilde{\omega}$ model and drawn by the field browser, with a: flow pattern, b: color filled flow field, c: color filled pressure field, d: color concentration contours, e: color filled $\widetilde{k}$ distribution and f: color filled $\widetilde{\omega}$ distribution, respectively. Figure 6d illustrates that the contaminant plume well develops along the left riverside at the lower reach of the tributary outlet section. $\widetilde{k}$ $\widetilde{k}-\widetilde{\varepsilon}$ $\widetilde{k}-\widetilde{w}$ Figures 7a, 7b and 7c demonstrate the 3D distributions of $\widetilde{k}$, calculated by using these three turbulence models and drawn by the 3D browser. They are quite similar each other, with the maximum values: $0.622\,m^2/s^2$ for $\widetilde{k}-\widetilde{\omega}$ modeling (7a), $0.609\,m^2/s^2$ for $\widetilde{k}-\widetilde{\varepsilon}$ modeling (7b) and $0.608\,m^2/s^2$ for $\widetilde{k}-\widetilde{w}$ modeling (7c), respectively. Figures 8a, 8b and 8c present the 3D distributions of $\widetilde{\omega}$, $\widetilde{\varepsilon}$ and $\widetilde{w}$, which are different each other, because of the different definitions of the used second transported variables in current computations. Actually, the $\widetilde{\varepsilon}$ value, shown in Figure 8b, ranges only from 4.64e-6 to $0.0097\,m^2/s^3$; however, the $\widetilde{w}$ and $\widetilde{\omega}$ range from 7.82e-5 to $0.95/s^2$ and from 0.88e-2 to $0.9735/s$, shown in Figure 8c and Figure 8a respectively. Figures 9a, 9b and 9c illustrate the 3D distributions of effective viscosity $\widetilde{\mu}_{\omega}$, while the depth-averaged turbulent eddy viscosity $\widetilde{\mu}_t$ was calculated by using Eq. (2) for $\widetilde{k}-\widetilde{\omega}$ modeling (9a), Eq. (9) for $\widetilde{k}-\widetilde{\varepsilon}$ modeling (9b) and Eq. (14) for $\widetilde{k}-\widetilde{w}$ modeling (9c), respectively. Basically, they are similar each other, specially for $\widetilde{k}-\widetilde{\varepsilon}$ and $\widetilde{k}-\widetilde{w}$ modeling, while the maximum values of $\widetilde{\mu}_{\omega}$ are $6260.4\,Pa.s$ (9b) and $6257.4\,Pa.s$ (9c); but the same value for $\widetilde{k}-\widetilde{\omega}$ modeling is $6313.7\,Pa.s$ (9a).

Figure 10 shows the distributions of the production term of turbulent kinetic energy, with the maximum values of P_k $3.15\,Pa.m/s$ for $\widetilde{k}-\widetilde{\omega}$ modeling (10a), $3.11\,Pa.m/s$ for $\widetilde{k}-\widetilde{\varepsilon}$

modeling (10b) and $3.11 Pa.m/s$ for $\widetilde{k} - \widetilde{w}$ modeling (10c). They are also similar each other. Figures 11a and 11b display the comparisons of concentration profiles along the centers of the volume cells at i from 1 to 258 and $j=32$ (*i.e.,* along a curved line from the inlet to the outlet near the north and east riverside) and at $i=230$ and j from 1 to 34 (*i.e.,* along a transversal section of $i=230$, which crosses the smaller island) on the fine grid, calculated by three $\widetilde{k} - \widetilde{\varepsilon}$ $\widetilde{k} - \widetilde{w}$ $\widetilde{k} - \widetilde{\omega}$ models. Figures 12a and 12b show the comparisons between $\widetilde{\varepsilon}$, $\widetilde{w}$ and $\widetilde{\omega}$ at the same centers of the fine grid. It is well known that the orders of magnitudes of $\widetilde{\varepsilon}$, $\widetilde{w}$ and $\widetilde{\omega}$, used in three turbulence models, have significant differences in deed.

Fig-6. A part of results, calculated by $\widetilde{k} - \widetilde{\omega}$ model.

a

b

c

d
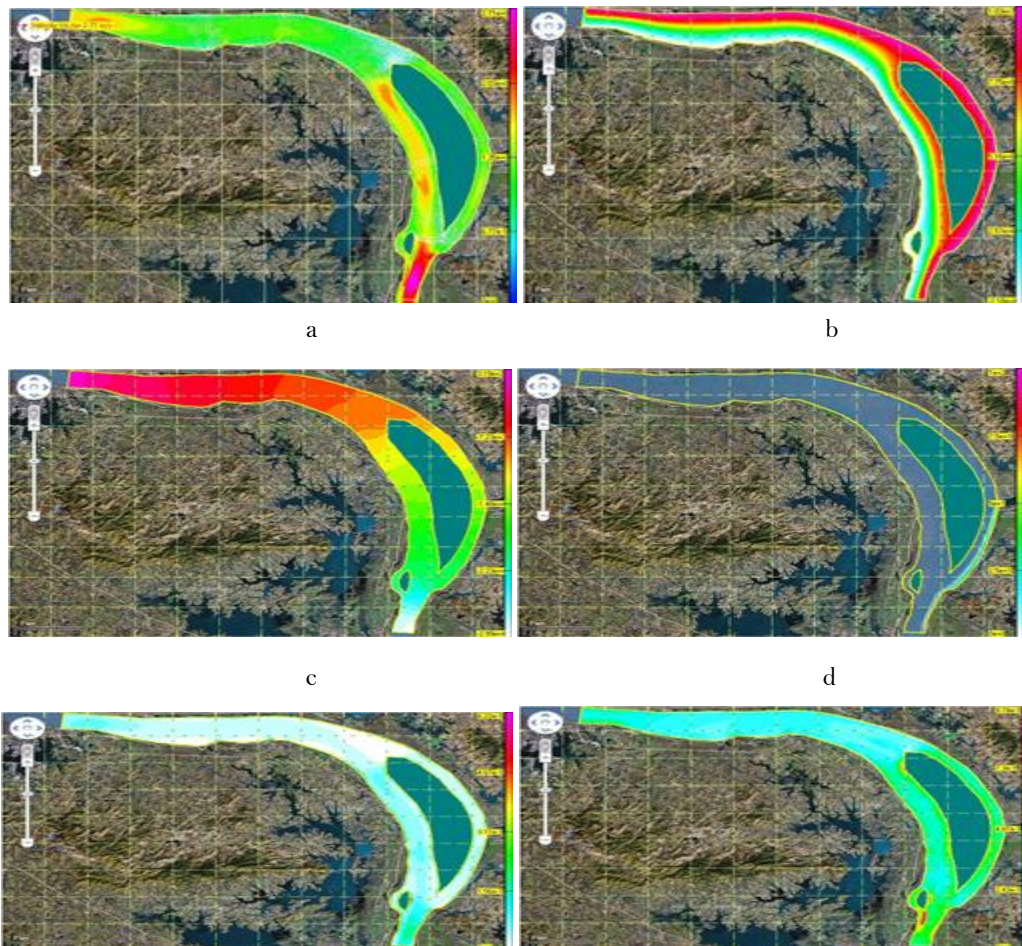
Fig-7. 3D $\widetilde{k}$ distributions, calculated by $\widetilde{k}-\widetilde{\omega}$, $\widetilde{k}-\widetilde{\varepsilon}$ and $\widetilde{k}-\widetilde{w}$ models.

a   b   c
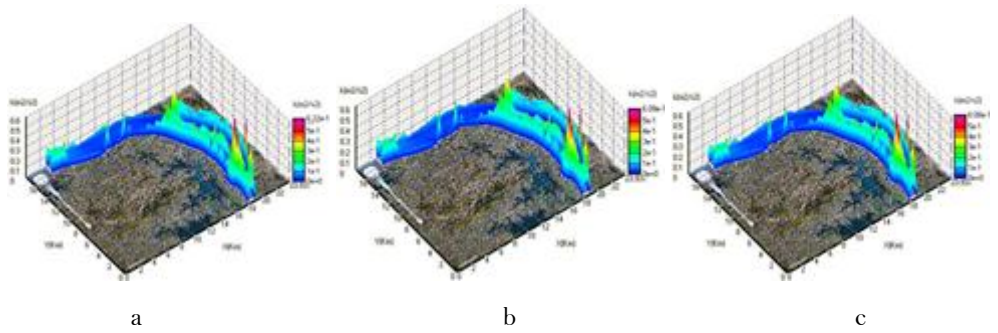
Fig-8. 3D $\widetilde{\omega}$, $\widetilde{\varepsilon}$ and $\widetilde{w}$ distributions.

a   b   c

Fig-9. 3D $\widetilde{\mu}_{\omega}$ distributions, calculated by $\widetilde{k}-\widetilde{\omega}$, $\widetilde{k}-\widetilde{\varepsilon}$ and $\widetilde{k}-\widetilde{w}$ models.

a   b   c
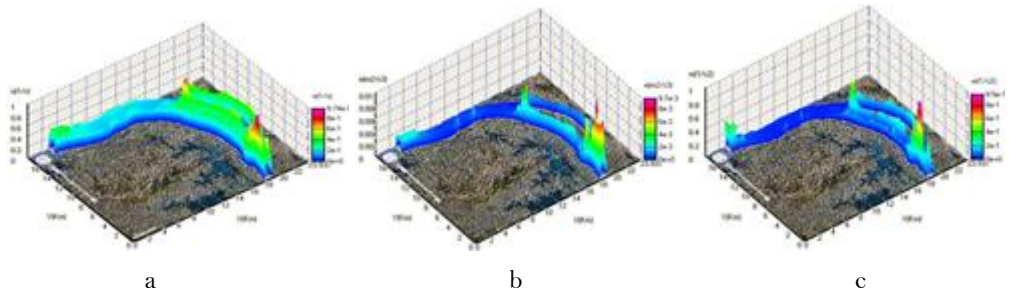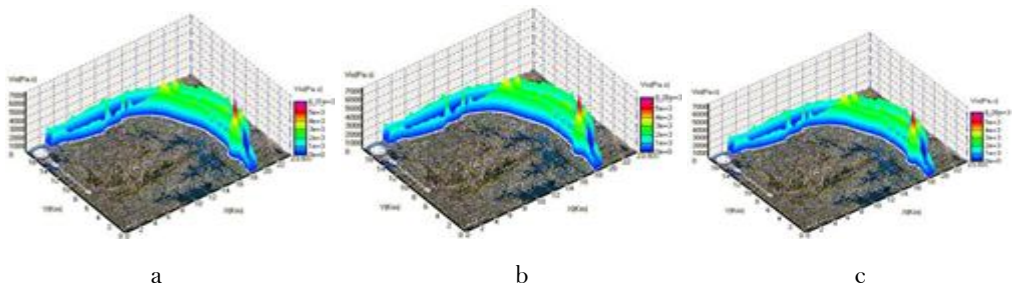
Fig-10. P_k distributions, calculated by $\widetilde{k}-\widetilde{\omega}$, $\widetilde{k}-\widetilde{\varepsilon}$ and $\widetilde{k}-\widetilde{w}$ models

a   b   c

12
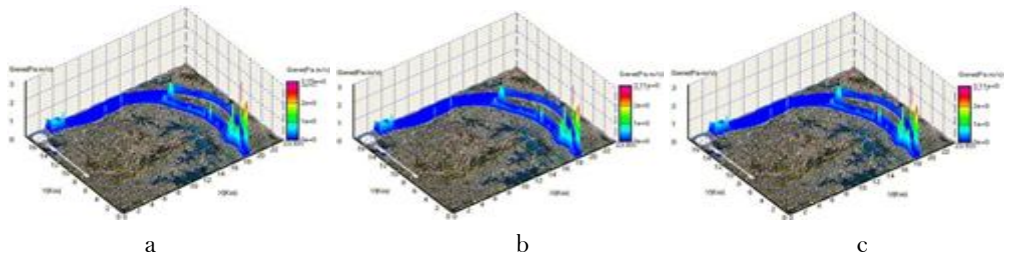
Fig-11. Concentrations at a: i from 1 to 258 and j=32; b: i=230 and j from 1 to 34.

a   b
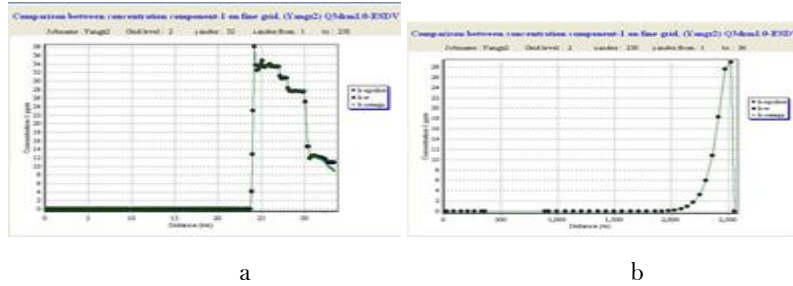
Fig-12. $\widetilde{\omega}$, $\widetilde{\varepsilon}$ and $\widetilde{w}$ at a: i from 1 to 258 and j=32; b: . i=230 and j from 1 to 34.

a   b
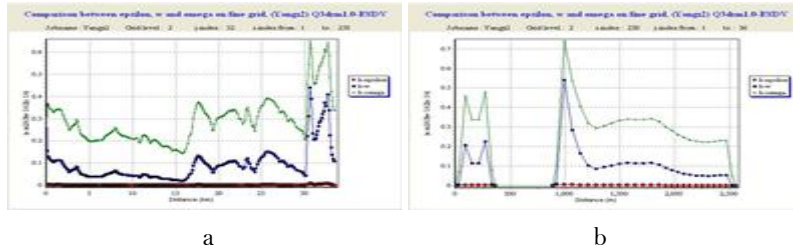
6. CONTAMINANT PLUME DEVELOPMENT AT THE BEGINNING OF DISCHARGE

In order to well understand the development process of pollutant plume, a special simulation was performed by using $\widetilde{k} - \widetilde{\omega}$ model for the case described as follows. Supposing the contaminant concentration of the tributary firstly to equal zero, and then, the value of concentration instantaneously reaches $100 mg/L$ at $Time$=0, while the flow-rates, either of main stream or of tributary, keep constant. Figures 13a-f illustrate the plume development and variation in the lower reach of tributary outlet section, where Figure 13a presents the situation of clean water confluence; Figures 13b-f display the process of contaminant inpouring and plume development, with an equal time difference Δt each other.

Fig-13. Contaminant plume development.

a Case 1, ΔC=0, $Time$=0   b Case 2, ΔC=$100mg/L$, $Time$=Δt

13

c Case 3, ΔC=*100mg/L, Time=2Δt*   d Case 4, ΔC=*100mg/L, Time=3Δt*
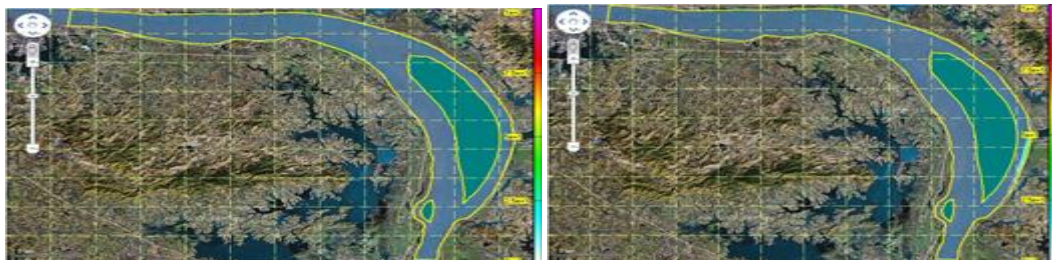
e Case 5, ΔC=*100mg/L, Time=4Δt*   f Case 6, ΔC=*100mg/L, Time=5Δt*
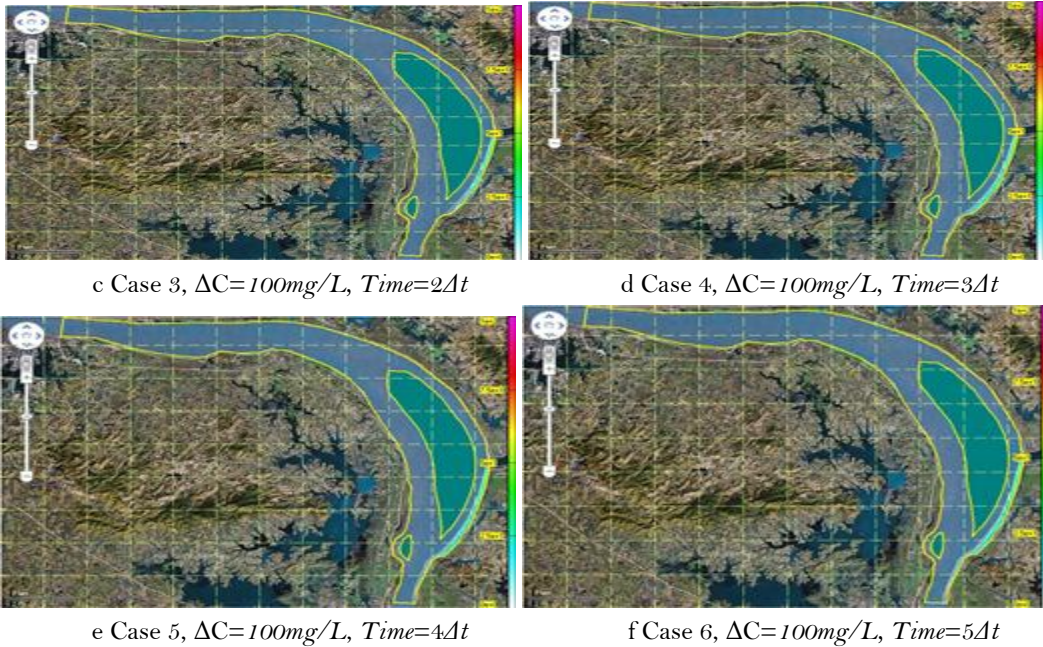
7. DISCUSSIONS AND CONCLUSIONS

Two-equation models are one of the most common types of turbulence closure models. The so-called 'standard' two-equation turbulence models, adopted widely in industry, cannot be directly used in depth-averaged modeling. Till now, the vast majority of quasi 3D numerical tools in the world only can provide depth-averaged $\tilde{k} - \tilde{\varepsilon}$ turbulence model, which appears already beyond 30 years. However, current advanced commercial Computational Fluid Dynamics (CFD) software for 'standard' 2D and 3D modeling can provide several, even up to dozens of two-equation closure turbulence models, because there is non-existent a 'universal' turbulence closure model in the theory of turbulence modeling. Moreover, two-equation turbulence models are also very much still an active area of research and new refined models are still being developed indeed. This situation should be changed as soon as possibly.

At present, the k-ω model, just like the k-ε model, has become industry standard model and is commonly used for most types of engineering problems. Therefore, the establishment of depth-averaged $\tilde{k} - \tilde{\omega}$ turbulence model and numerical investigation as well as comparison with existing depth-averaged turbulence models are significant.

Two levels' grids were used in this simulation. The simulation on these two grids can satisfy the simulation demand. If it is necessary, by setting the number of grid levels at three in the developed software, for example, the computations not only on coarse and fine grids but also on finest grid can be realized. The selection of the number of grid levels depends on the solved problems and computational requirements.

14

The solved depth-averaged concentration variable in the current computation is the contaminant concentration difference between the confluent tributary and main stream ($100mg/L$). However, other indexes of the discharged contaminant, such as COD and BOD, also can be considered as the solved variable. The developed software possesses the ability to simultaneously solve two concentration components in once calculation, which may be caused by industrial, domestic, and natural discharges.

Figure 7 demonstrates that the distributions of $\widetilde{k}$, calculated by three turbulence models, vary strongly in the computational domain, but quite similar to one another. However, the characteristics of the distributions of $\widetilde{\varpi}$, $\widetilde{\varepsilon}$ and $\widetilde{w}$, shown in Figures 8a, 8b and 8c, respectively, are different from one another, though they also vary sharply. The calculated effective viscosity $\widetilde{\mu}_{e\!f\!f}$, presented in Figures 9a, 9b and 9c, also varies strongly. In fact, the eddy viscosity changes from point to point in the computational domain, especially in the areas near the riversides and boundaries of islands. To solve the problems of contaminant transport caused by side discharge, for example, the plume usually develops along a region near riverside (see Figure 6d and Figure 13), where $\widetilde{\mu}_{t}$ (or $\widetilde{\mu}_{e\!f\!f}$) actually varies much strongly (see Figure 9). This means that $\widetilde{\mu}_{t}$ should be precisely calculated using suitable higher-order turbulence closure models with higher precision, and cannot be simply considered as an adjustable constant.

Figure 11 shows that the concentration profiles along the north and east riverbank, either calculated by $\widetilde{k}-\widetilde{\varpi}$ and $\widetilde{k}-\widetilde{\varepsilon}$ closures, or calculated by $\widetilde{k}-\widetilde{w}$ closure, only have a quite small difference from one another. This means that three utilized turbulence models almost have the same ability to simulate plume distributions along riverbank. This conclusion also coincides with the result of author's previous research that the depth-averaged two-equation turbulence models are suitable for modeling strong mixing turbulence [24]. However, the abilities and behaviors of different depth-averaged turbulence models for rather weak mixing, also often encountered in engineering, should be further investigated.

Except for the different definitions of transported variables: $\widetilde{\varepsilon}$, $\widetilde{w}$ and $\widetilde{\varpi}$, the order of magnitude of $\widetilde{\varepsilon}$ is smaller than the order of magnitude of $\widetilde{w}$, and much smaller than the order of magnitude of $\widetilde{\varpi}$. It should be noticed that three transported variables: $\widetilde{\varepsilon}$, $\widetilde{w}$ and $\widetilde{\varpi}$ all appear in the denominators of Eqs. (9), (14) and (2), which were used to calculate turbulent eddy viscosity

15

$\widetilde{\mu}_t$. For numerical simulation, the occurrence of numerical error is unavoidable, especially in the region near irregular boundary. It is clear that a small numerical error, caused by solving $\widetilde{\varepsilon}$ -eq, for example, will bring on larger error for calculating eddy viscosity than the same error caused by solving the other two equations (*i.e.*, the $\widetilde{w}$ -eq. and $\widetilde{\omega}$ -eq.). Without doubt, the elevation of the order of magnitude of the used second turbulent variable, reflecting the advance of two-equation turbulence models, provides a possibility for users to improve their computational precision. The insufficiency of traditional depth-averaged $\widetilde{k} - \widetilde{\varepsilon}$ model may be avoided by adopting other turbulence models that have appeared recently, such as the $\widetilde{k} - \widetilde{\omega}$ model.

The developed GUI of **Q3drm1.0** can be used in various Windows-based microcomputers. The pre- and post-processors of this tool, supported by a powerful self-contained map support tool together with a detailed help system, can help the user to easily compute the flows and contaminant transport behaviors in natural waters, closed by using three depth-averaged two-equation turbulence models, and to draw and analyze various 2D and 3D graphics of computed results.

8. ACKNOWLEDGEMENT

REFERENCES

[1]   M. Choi and H. Takashi, "A numerical simulation of lake currents and characteristics of salinity changes in the freshening process," *J. Japan Society of Hydrology and Water Resources, (In Japanese)*, vol. 13, pp. 439-452, 2000.

[2]   M. Lunis, V. Mamchuk, V. Movchan, L. Romanyuk, and E. Shkvar, "Algebraic models of turbulent viscosity and heat transfer in analysis of near-wall turbulent flows," *International J. Fluid Mechanics Research. Available: http://dx.doi.org/doi/10.1615/InterJFluidMechRes.v31.i3.60*, vol. 31, pp. 60-74, 2004.

[3]   J. Vasquez, "Two dimensional finite element River morphology model," Ph. D. Dissertation, University of British Columbia, 2005.

[4]   S. Kwan, "A two dimensional hydrodynamic river morphology and gravel transport model," Master (MASc) Degree Thesis, University of British Columbia, 2009.

[5]   E. Viparelli, O. Sequeiros, A. Cantelli, P. Wilcock, and G. Parker, "River morphodynamics with creation/consumption of grain size stratigraphy 2: Numerical model," *Journal of Hydraulic Research. Available: http://dx.doi.org/doi/doi:10.1080/00221686.2010.526759*, vol. 48, pp. 727-741, 2010.

[6]   W. Rodi, R. Pavlovic, and S. Srivatsa, *Prediction of flow pollutant spreading in rivers. In: Transport models for inland and coastal waters: Proceedings of the symposium on predictive ability.* Berkeley: University of California Academic Press, 1980.

[7]   R. Chapma and C. Kuo, "A numerical simulation of two-dimensional separated flow in a symmetric open-channel expansion using the depth-Integrated two equation (k-ε) turbulence closure model. Rep. 8202," Virginia Polytechnic Inst. and State Univ., Blacksburg, VA1982.

[8]   Z. Mei, A. Roberts, and Z. Li, "Modeling the dynamics of turbulent floods," *SIAM J. Applied Mathematics. Available: http://dx.doi.org/doi/10.1137/S0036139999358866*, vol. 63, pp. 423-458, 2002.

[9]   H. Johnson, T. Karambas, I. Avgeris, B. Zanuttigh, D. Gonzalez-Marco, and I. Caceres, "Modelling of waves and currents around submerged breakwaters," *Coastal Engineering. Available: http://dx.doi.org/doi/10.1016/j.coastaleng.2005.09.011*, vol. 52, pp. 949-969, 2005.

[10]   L. Cea, L. Pena, J. Puertas, M. Vazquez-Cendon, and E. Pena, "Application of several depth-averaged turbulence models to simulate flow in vertical slot fishways," *J. Hydraulic Engineering. Available: http://dx.doi.org/doi/10.1061/(ASCE)0733-9429(2007)133:2(160)*, vol. 133, pp. 160-172, 2007.

[11]   Z. Hua, L. Xing, and L. Gu, "Application of a modified quick scheme to depth-averaged κ–ε turbulence model based on unstructured grids," *J. Hydrodynamics Ser. B.*, pp. 514-523, 2008.

[12]   I. Kimura, W. Uijttewaal, T. Hosoda, and M. Ali, "URANS computations of shallow grid turbulence," *J. Hydraulic Engineering. Available: http://dx.doi.org/doi/10.1061/(ASCE)0733-9429(2009)135:2(118)*, vol. 135, pp. 118-131, 2009.

[13]   J. Lee, H. Chan, C. Huang, Y. Wang, and W. Huang, "A depth-averaged two-dimensional model for flow around permeable pile groins," *International J. the Physical Sciences. Available: http://dx.doi.org/doi/10.5897/IJPS11.078*, vol. 6, pp. 1379-1387, 2011.

[14]   L. Yu, *Quasi 3D modeling flow and contaminant transport in shallow waters.* Germany: Lap Lambert Academic Publishing, 2013.

[15]   J. Ferziger and M. Peric, *Computational methods for fluid dynamics*, 3rd ed. Berlin: Springer, 2002.

[16]   P. Saffman, *A model for inhomogeneous turbulent flow* vol. A317. London: In: Proc. Roy. Soc., 1970.

[17]   D. Wilcox, *Turbulence modeling for CFD.* La Canada: DCW Industries, Inc., 1998.

[18]   A. Riasi, A. Nourbakhsh, and M. Raisee, "Unsteady turbulent pipe flow due to water hammer using k–ω turbulence model," *J. of Hydraulic Research. Available: http://dx.doi.org/doi/10.1080/00221681003726247*, vol. 47, pp. 429-437, 2009.

[19]   M. Kirkgoz, M. Akoz, and A. Oner, "Numerical modeling of flow over a chute spillway," *J. Hydraulic Research*, vol. 47, pp. 790-797, 2009.

[20]   L. Yu and J. Yu, "Numerical research on flow and thermal transport in cooling pool of electrical power station using three depth-averaged turbulence models," *Water Science and Engineering. Available: http://dx.doi.org/doi/10.3882/j.issn.1674-2370.2009.03.001*, vol. 2, pp. 1-12, 2009.

[21]   J. McGuirk and W. Rodi, *A depth-averaged mathematical model for side discharges into open channel flow.* SFB 80/T/88. Germany: Universität Karlsruhe, 1977.

[22]   L. Yu and S. Zhang, "A new depth-averaged two-equation (k-w) turbulent closure model," *J. Hydrodynamics Series. B.,* vol. 1, pp. 47-54, 1989.

[23]   J. Ilegbusi and D. Spalding, *Application of a new version of the K-W model of turbulence to a boundary layer with mass transfer.* CFD/82/15. London: Imperial College, 1982.

[24]   L. Yu and A. Righetto, "Depth-averaged turbulence model and applications," *Advances in Engineering Software. Available: http://dx.doi.org/doi/10.1016/S0965-9978(00)00100-9,* vol. 32, pp. 375-394, 2001.